The Role of Cavitation in Liposome Formation

Eric S. Richardson,* William G. Pitt,† and Dixon J. Woodbury‡
*Department of Biomedical Engineering, University of Minnesota, Minneapolis, Minnesota; and †Department of Chemical Engineering, and ‡Department of Physiology and Developmental Biology, Brigham Young University, Provo, Utah

ABSTRACT Liposome size is a vital parameter of many quantitative biophysical studies. Sonication, or exposure to ultrasound, is used widely to manufacture artificial liposomes, yet little is known about the mechanism by which liposomes are affected by ultrasound. Cavitation, or the oscillation of small gas bubbles in a pressure-varying field, has been shown to be responsible for many biophysical effects of ultrasound on cells. In this study, we correlate the presence and type of cavitation with a decrease in liposome size. Aqueous lipid suspensions surrounding a hydrophone were exposed to various intensities of ultrasound and hydrostatic pressures before measuring their size distribution with dynamic light scattering. As expected, increasing ultrasound intensity at atmospheric pressure decreased the average liposome diameter. The presence of collapse cavitation was manifested in the acoustic spectrum at high ultrasonic intensities. Increasing hydrostatic pressure was shown to inhibit the presence of collapse cavitation. Collapse cavitation, however, did not correlate with decreases in liposome size, as changes in size still occurred when collapse cavitation was inhibited either by lowering ultrasound intensity or by increasing static pressure. We propose a mechanism whereby stable cavitation, another type of cavitation present in sound fields, causes fluid shearing of liposomes and reduction of liposome size. A mathematical model was developed based on the Rayleigh-Plesset equation of bubble dynamics and principles of acoustic microstreaming to estimate the shear field magnitude around an oscillating bubble. This model predicts the ultrasound intensities and pressures needed to create shear fields sufficient to cause liposome size change, and correlates well with our experimental data.

INTRODUCTION

Liposome size is a vital parameter of many quantitative biophysical studies, of liposomal drug delivery studies, and of many other applications in both medicine and biology (1–4). Several methods have been developed to manipulate the size of manufactured liposomes such as detergent dialysis (5), extrusion (6,7), alcohol injection (8), and sonication (exposure to ultrasound) (9). Although sonication has been used since the 1960s, little is known about the mechanism by which the average liposome size decreases with exposure to ultrasound. It has been postulated that ultrasonic energy randomly and uniformly shatters larger liposomes into smaller discoid sections called bilayer phospholipid fragments or BPFs (10–12). These fragments fold up into thermodynamically stable liposomes.

Cavitation, a principal effect of low-frequency sonication, has been shown to be responsible for many biophysical effects of ultrasound on cells (13). Acoustic cavitation is the expansion and contraction of gas bubbles in a liquid exposed to acoustic pressure waves. Repeatable bubble oscillation without implosion is called ''stable cavitation'' and is present at low intensities of ultrasound or when the resonance frequency of the bubble is far from the applied frequency. As ultrasound intensity increases, bubbles whose size is near the resonant size for the applied frequency begin to oscillate nonlinearly and eventually collapse. The collapse results in a violent implosion that produces extremely high temperatures, high pressures, free radicals, and shock waves (14). This type of cavitation is called transient, inertial, or collapse cavitation. Given a distribution of bubbles exposed to ultrasound, some will experience stable cavitation, whereas other bubbles may undergo collapse cavitation.

Both types of cavitation can be detected by analyzing the acoustic radiation emanating from the bubble(s). Stable cavitation is evidenced by the radiation of the fundamental, higher harmonic, and sometimes subharmonic frequencies (14–16). There is still some debate as to the origin of the subharmonic frequencies. Collapse cavitation has been correlated with the presence of a strong subharmonic frequency and additional noise in the baseline of the sound spectrum, called broadband emission (14). Acoustic radiation due to cavitation phenomena can be substantially reduced by raising the static pressure of the liquid medium. This technique has been used previously to inhibit some of the bioeffects of ultrasound (17,18).

By using pressure to inhibit cavitation and by listening to bubble acoustic spectra to detect various cavitation modes, this study explores the role of cavitation in manipulating liposome size. We hypothesize that ultrasonic cavitation phenomena play a key role in altering the size distribution of liposomes processed in an ultrasonic bath. By correlating changes in liposome size with cavitation emissions at various acoustic intensities and static pressures, the role of the cavitating bubble in liposome size manipulation is explored.

Submitted February 8, 2007, and accepted for publication July 6, 2007.

Address reprint requests to Dr. Dixon Woodbury, 574 WIDB, Brigham Young University, Provo, UT 84602. Tel.: 801-422-7562; E-mail: dixon_woodbury@byu.edu.

Editor: Marileen Dogterom.

0006-3495/07/12/4100/08 $2.00

doi: 10.1529/biophysj.107.104042

METHODS

Liposome preparation

Liposomes were prepared before sonication using detergent dialysis. *Escherichia coli* polar lipid extract (Avanti Polar Lipids, Alabaster, AL) was added to an *n*-octyl β-D-glucopyranoside solution and dialyzed as described previously (19).

Experimental apparatus

An apparatus was built to listen to the liposome sample (and not the coupling medium) under various ultrasound intensities and hydrostatic pressures. An 80-kHz cylindrical bath sonicator (Laboratory Supplies Company, Hicksville, NY) was used to generate the ultrasound. This is a common sonicating bath used to prepare liposome suspensions for biophysical studies (20,21). The bath was powered by a variable AC transformer that allowed us to change the voltage supplied to the bath and thus vary the intensity of the ultrasound. The bath produced pulses of 80-kHz ultrasound at a 60-Hz repetition frequency and a duty cycle of ~50%. Samples were sonicated at three intensities of ultrasound: low (~0.01 W/cm^2), medium (~0.04 W/cm^2), and high (~0.07 W/cm^2). The three intensities were purposefully chosen so that low intensity would have present neither the subharmonic nor broadband emission, medium intensity would have the subharmonic present but only a small amount of broadband emission, and high intensity would have the subharmonic and a large amount of broadband emission.

As seen in Fig. 1, the sample was suspended in the center of the bath by a tube mounted under the lid. The sample was contained within a thin-walled polyethylene bulb, which is nearly transparent to ultrasound. Water (450 ml) was added to the ultrasonic bath before each experiment so that the bulb was always immersed 18 mm below the water surface. Mounted inside the bulb was a hydrophone (8103, Bruel & Kjaer, Nærum, Denmark) enabling us to listen inside the sample. The bulb was pressurized with compressed air via a small tube entering the bulb adjacent to the hydrophone, and pressure was controlled with a pressure regulator. Samples were sonicated at 1 atm, 2 atm, and 4 atm (absolute pressure).

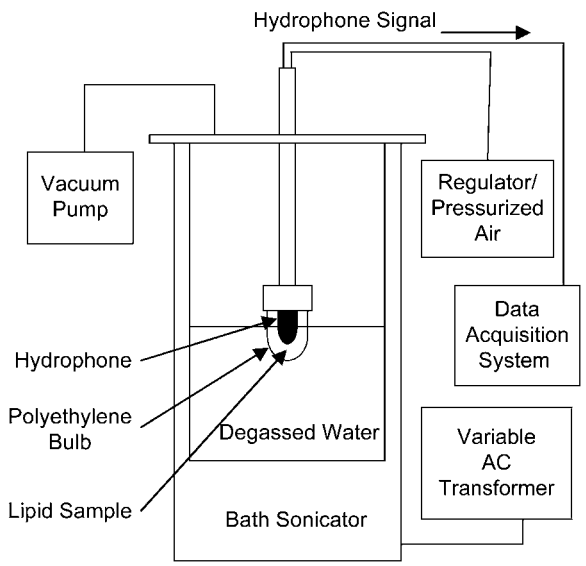

FIGURE 1 Experiment apparatus. A bath sonicator powered by a variable AC transformer provided various intensities of ultrasound. The lipid suspension surrounding the hydrophone was contained in a small polyethylene bulb. An inlet at the top of the bulb allowed the sample to be pressurized. The lid sealed with the bath so that a vacuum could be drawn to degas the coupling water before each experiment.

Special care was taken to prevent impurities or dissolved gas from nucleating cavitation bubbles in the water surrounding the sample and thus interfering with the acoustic signal from the sample. The water used in the bath was distilled, deionized to a resistivity of 18 MΩ (ZyzaTech, Kent, WA), and set in an incubator at 40°C for at least 6 h to partially degas. The water was changed in the bath before every experimental run. The lid was sealed on the top of the bath with a gasket, allowing us to draw a vacuum over the surrounding water while the sample was in place. To provide a final degasification of the surrounding water, a vacuum pump connected to the lid was run for 1 min immediately before each sample was sonicated.

After each sample had been sonicated, sample temperature was measured by a thermocouple within ~1 min. Typically, there was only a slight increase in temperature, however at higher ultrasound intensities, temperatures increased ~10°C (after 15 min of continuous processing). The lipids used were already above their phase transition temperature at room temperature, so no phase change took place during sonication. Therefore, we assume that thermal effects on liposome stability were minimal in our experiments.

The signal from the hydrophone was sampled using a Microstar Labs data acquisition card (Bellevue, WA) at a rate of 491,000 samples/s. The Fourier transform of the digitized signal was calculated with DASYLab software (DasyTech USA, Bedford, NH). Thirty Fourier transforms were collected and mean-averaged every 8 s. Averages were saved to disk and analyzed as described below.

Real-time light microscopy images of liposome suspensions were collected using the real-time microscopy (RTM)-3 technology (Richardson Technologies, Toronto, Ontario, Canada), which enhances conventional light microscopy. The objective used for this work was an infinity-corrected, 100×, 1.4-NA, 0.17-coverslip, oil-immersion objective with plan-apochromatic correction. The depth of field of the RTM images collected using the 100× objective was 320 nm. The images were acquired using a Datacell Snapper 24-image capture card (Datacell, Finchampstead, UK) and OpenLab Version 3.1.5 software (Improvision, Coventry, UK).

Fourier transform analysis

The fast Fourier transform (FFT) data were analyzed using our own custom MATLAB codes (The MathWorks, Natick, MA). In this study, we were interested in two components of the FFT: the magnitude of the broadband emission, and the integrated area of the subharmonic peak. To find the magnitude of the broadband emission, the FFT data were sorted by magnitude, and then the average of the lowest 25% of the values was taken. This algorithm provided a value that matched the ''eyeball'' or graphical estimate of the baseline in preliminary experiments. Integration of the subharmonic peak was performed by identifying the maximum amplitude within a certain frequency window (near 40 kHz), and then integrating over a predetermined width (10 kHz) centered on the frequency of the greatest amplitude. The appropriate area of integration of the broadband emission was subtracted from the peak integration to give a final adjusted peak area. The fundamental emission (near 80 kHz) was integrated in a similar way. Fig. 2 shows an example of the broadband emission magnitude and the limits of integration as chosen by the custom MATLAB software. The other peaks in Fig. 2 are fold-back peaks artificially generated by the numerical FFT of the digitized acoustic waveform. Although analog filtering was used, some (attenuated) fold-back peaks could not be avoided; therefore the fold-back (Nyquist) frequency was carefully selected such that none of these fold-back peaks were in the 40 kHz or 80 kHz window.

Dynamic light scattering

All aliquots of lipid solutions were first sonicated in the (pressurized) bulb for 100 s, after which 100 μL were sampled for dynamic light scattering (DLS) measurements. Following this sampling, sonication was resumed on the same aliquot for an additional 900 s, producing a total of 1000 s of sonication. Immediately thereafter, 100 μL of lipid solution were sampled for sizing.

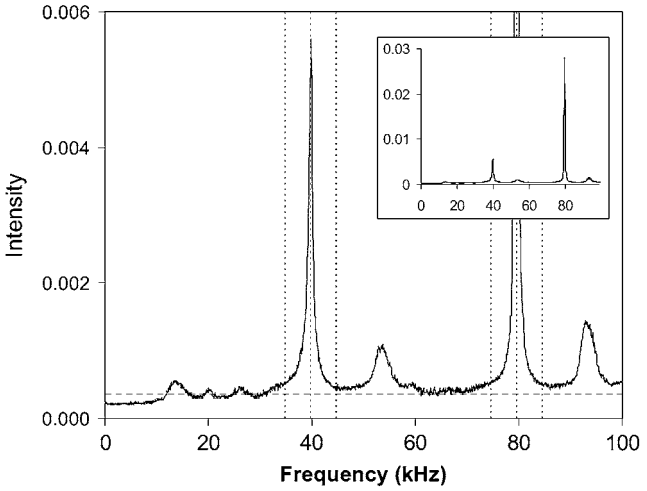

FIGURE 2 Example of MATLAB Analysis of FFT data. The magnitude of the broadband emission (arbitrary units) and limits of integration of the fundamental (at 80 kHz) and the subharmonic (at 40 kHz) used by MATLAB are shown by the dotted lines. The inset is the same data on a larger y axis range.

Three 30 μL volumes were taken from every 100 μL sample and were each diluted using their original buffer (150 mM KCl) in a 4-mL cuvette. All DLS measurements were performed at a scatter angle of 90° using a Brookhaven 90Plus particle sizer (Brookhaven Instruments, Holtsville, NY). Preliminary measurements at 15° detected an insignificant amount of scatter due to large (multimicron) particles. All parameters and algorithms used were previously reported (20). Each cuvette was analyzed by performing ten 1-min ''runs'', totaling 30 min for each 100-μL sample obtained for sizing. The data from the first two 1-min runs, which, based upon previous experience, tend to be inconsistent with the final 8 min of data, were discarded. An effective diameter, d, was calculated by the software directly from the measured translational diffusion coefficient, D, according to the equation $d = k_B T/(3\pi\mu D)$, where k_B is Boltzmann's constant, T is the temperature, and μ is the viscosity of the fluid (water). The NNLS (nonnegative least squares) algorithm (22) makes no assumptions as to the shape of the distribution, and therefore can predict the modality of the population. The NNLS algorithm was also executed on the ensemble of eight 1-min samples. The adjusted average of the three 8-min ensembles was mean-averaged and a standard error of the mean was calculated.

Numerical modeling of bubble dynamics

The Rayleigh-Plesset equation for spherical bubble dynamics was used to model the bubble behavior in the acoustic field (15):

$$\frac{p_v(T_\infty) - p_\infty(t)}{\rho_L} + \frac{p_{G_O}}{\rho_L}\left(\frac{R_O}{R(t)}\right)^{3k} = R(t)\ddot{R}(t) + \frac{3}{2}(\dot{R}(t))^2 + \frac{4\nu_L\dot{R}(t)}{R(t)} + \frac{2S}{\rho_L R(t)}, \quad (1)$$

TABLE 1 Constants used in the Rayleigh-Plesset equation

$p_v(T_\infty)$	= vapor pressure of liquid at $T_\infty = 2.34 \times 10^3$ Pa
ρ_L	= density of liquid at $T_\infty = 998$ kg/m^3
k	= polytropic constant of air = 1.33
ν_L	= kinematic viscosity of water at $T_\infty = 1.0 \times 10^{-6}$ m^2/s
S	= surface tension of the gas/liquid interface = 0.073 N/m

where

$$p_{G_O} = p_\infty(0) - p_v(T_\infty) + \frac{2S}{R_O}, \quad (2)$$

and $p_v(T_\infty)$ = vapor pressure of liquid at T_∞ (the temperature away from the bubble), $p_\infty(t)$ = time-dependent pressure of the liquid, $p_\infty(0)$ = time invariant pressure away from bubble, ρ_L = density of the liquid, R_0 = initial bubble radius, $R(t)$ = time-dependent bubble radius, k = polytropic constant of enclosed gas, $\dot{R}(t) = dR(t)/dt$, $\ddot{R}(t) = d^2R(t)/dt^2$, ν_L = kinematic viscosity, and S = interfacial surface tension.

The values for some of these parameters are given in Table 1. All parameters were taken at room temperature and assumed to be constant throughout the duration of the experiment.

The dynamic behavior of the bubble radius as a function of time in stable cavitation was predicted using the ''ode45'' function of MATLAB, which uses both fourth- and fifth-order Runga-Kutta algorithms to determine an appropriate time step and to calculate the behavior. In all graphs shown, the bubble dynamics were calculated for the first 8300 μs (the entire ''on'' period of a pulse of ultrasound) of exposure to a sinusoidal pressure input. The initial conditions applied at $t = 0$ were that of the resting radius of the bubble and zero radial velocity.

RESULTS

Prepared samples were sonicated at three different static pressures: 1, 2, and 4 atm (absolute pressure) and three different acoustic intensities (0.01, 0.04, and 0.07 W/cm^2) for a total of nine sonicated samples. The effective mean diameters of each sample after both 100 and 1000 s of sonication are shown in Fig. 3.

At atmospheric pressure (1 atm), the expected trend of decreasing liposome size with longer sonication exposure is observed (20). Higher acoustic intensities produced smaller vesicles by the end of the 1000 s exposure. However, at higher pressures and lower acoustic amplitudes, the trend was inhibited. For example, at 2 atm, the vesicles exposed to the lowest-intensity ultrasound showed negligible size change, whereas the medium-intensity exposure still produced a small decrease (Fig. 3 *B*). At 4 atm, the decrease in vesicle size is almost completely inhibited at both low and medium acoustic intensities. Thus, size decrease is inhibited by raising the static pressure, but this inhibition can be moderated by increasing the ultrasonic intensity.

Fig. 4 shows the effects of pressurization on the presence of both the subharmonic and the broadband emission. As mentioned previously, these two components of the FFT are indicative of collapse cavitation. Note that pressurization eventually inhibits both components of the acoustic spectrum (see Fig. 4), and therefore inhibits cavitation, as previously reported (17). The sudden increase in the subharmonic intensity at high power density at 2 atm is an unexplained anomaly that was reproducible. We can only hypothesize that it is attributable to the dynamics of the bubbles in the system, and speculate that pressurization perhaps brings more bubbles close to resonant size.

An important correlation between Figs. 3 and 4 is that liposome size reduction occurred at 1 atm, with neither strong subharmonic nor broadband emission. In addition, the

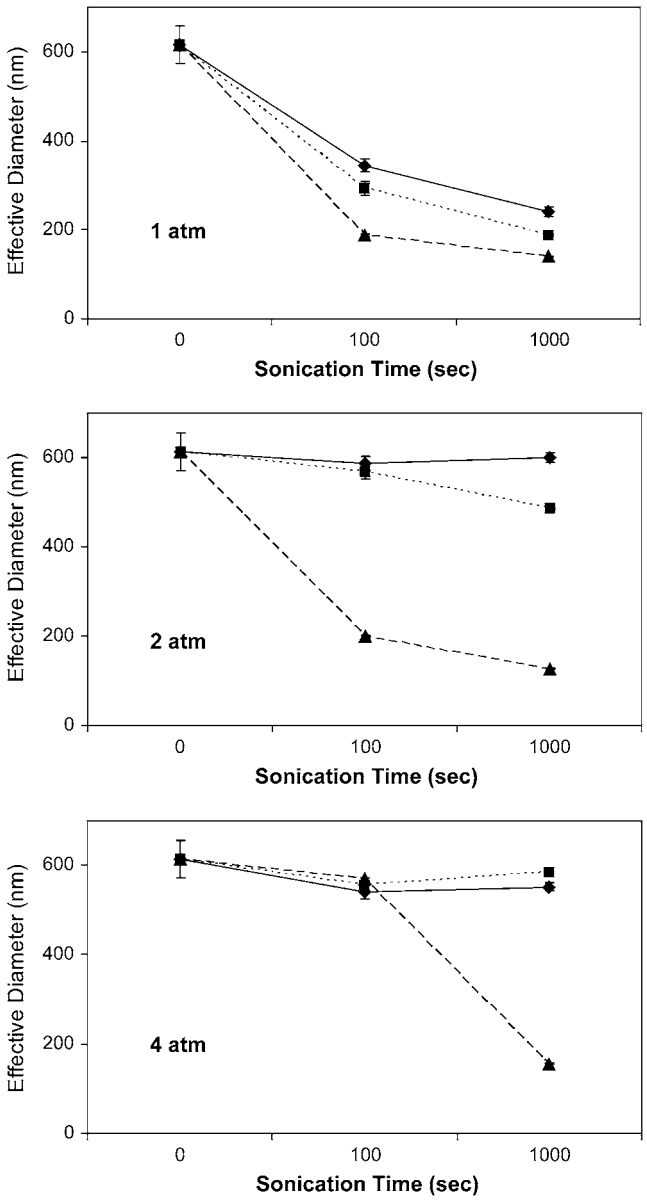

FIGURE 3 Effective diameter of sonicated liposomes at various intensities and hydrostatic pressures. The upper, middle, and lower plots show the effect of ultrasonication on liposome diameter at 1, 2, and 4 atm (absolute pressure), respectively. Low (♦, 0.01 W/cm^2), medium (■, 0.04 W/cm^2), and high (▲, 0.07 W/cm^2) intensities are shown on each graph. Note that as the hydrostatic pressure is increased, the effect of sonication on liposome size is inhibited. Higher intensity counteracts this inhibition.

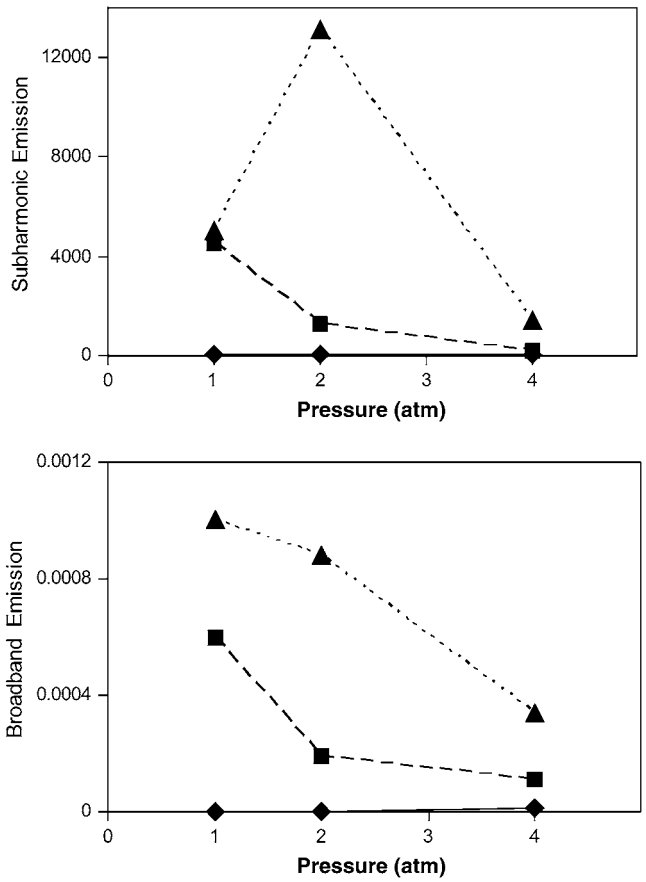

FIGURE 4 Subharmonic integration and broadband emission at various ultrasound intensities and hydrostatic pressures. The upper graph shows the eventual inhibition of the subharmonic at low (♦), medium (■), and high (▲) intensities by increasing hydrostatic pressure. The abnormally high increase in the subharmonic at 2 atm and high intensity is a repeatable yet unexplainable anomaly. In the lower graph, broadband emission is also inhibited with pressure. It is important to note that neither the subharmonic nor the broadband emission was present at low intensities, where size change was still seen.

presence of a subharmonic and broadband emission in medium and high intensities did not correspond to a drastically greater size reduction. These observations provide strong support that the subharmonic and broadband components of the acoustic spectrum are not correlated with decreasing liposome size.

It may seem odd that the subharmonic and broadband emissions are present at the low acoustic intensities used in this study. The threshold predicted by Apfel and Holland (23) is much higher than those we report. This may be caused by some of the lipids in our system acting as surfactants and lowering the cavitation threshold. In addition, whereas cavitation thresholds have been well defined for high-frequency diagnostic ultrasound, the low-frequency ultrasound used herein was at the low end of the frequency range used by Apfel and Holland to develop their models of the threshold of collapse cavitation. More importantly, their estimates of collapse-cavitation thresholds were based on pulses of <10 acoustic cycles (23); yet in this work, the pulse is on the order of 700 cycles, which allows much more time to excite the bubbles to nonlinear behavior.

Deconvolution of the DLS signal with the NNLS algorithm showed that those samples that exhibited a significant size reduction typically had a distinct bimodal population distribution. We have observed this phenomenon previously with mildly sonicated liposomes, using three independent

techniques to verify this bimodality (20). Any model of vesicle size reduction due to cavitation must also account for this bimodality.

DISCUSSION AND MATHEMATICAL MODEL

We have shown that increased static pressure, which inhibits both stable and collapse cavitation, also suppresses the effects of sonication intensity in decreasing liposome size. However, the classic indicators of collapse cavitation, the presence of a subharmonic and broadband emission, do not correlate with liposome size change. The absence of the subharmonic and broadband emission does not imply that all cavitation is absent; any gas bubble within a sound field will oscillate to some degree and produce some stable cavitation. Neither does the observation of broadband emission (and therefore collapse cavitation) imply that stable cavitation is absent. Because there is a distribution of sizes of gas bubbles in these lipid solutions, some amount of stable cavitation will always be present during sonication, no matter the intensity.

Thus the absence of collapse cavitation does not imply the absence of strong forces in the lipid solution. Seemingly small, stable oscillations can have surprisingly large effects on nearby particles such as cells or liposomes (14,15,24–26). Sound radiating from an oscillating bubble creates a local pressure force (called the radiation pressure) which draws toward the bubble any particle whose density is greater than that of the surrounding liquid (27,14). Since these liposomes can be pelleted, they are denser than their surroundings and will be driven toward the bubbles by radiation pressure.

As the bubble's radius expands and contracts on the timescale of microseconds, convective flow patterns develop near the surface of an oscillating bubble. The collection of convective flow patterns produced by the oscillating bubble is termed ''acoustic microstreaming'' (24,26,27). Such microstreaming exposes the attracted particles to extremely high shear rates near the bubble surface. Wu has shown that these shear forces are strong enough to perforate cell membranes in the absence of any collapse cavitation (28). We propose that these localized and very high shear rates are the cause for the reduction in liposome size (20).

To determine the magnitude of the shear caused by stable cavitation, the maximum wall velocities of the oscillating bubbles at various power densities were calculated using the Rayleigh-Plesset equation (Eq. 1). The original bubble size distribution in the experiments was not known, but we assumed that there were some bubbles near resonant size, and that they are responsible for the majority of the shear forces. For example, the Rayleigh-Plesset equation indicates that wall velocities of bubbles near resonant size are at least an order of magnitude greater than velocities of bubbles 10 times smaller or larger in diameter. Similarly, Wu has shown theoretically that the shear generated by albumin-coated microbubbles is largely dependent on size (28). The resonant bubble size (R_o) was calculated using the following equation developed by Phelps (29):

$$f_0 = \frac{1}{2\pi R_0\sqrt{\rho_L}}\left[3k\left(P_0 + \frac{2S}{R_0}\right) - \frac{2S}{R_0} - \frac{4\mu^2}{\rho_L R_0^2}\right]^{1/2}, \quad (3)$$

where μ = liquid viscosity (=.001 kg/(m × s) for water), P_0 = static pressure of the liquid, f_o = resonant frequency, and all other terms are as defined previously.

According to Eq. 3, the resonant bubble diameter at 1 atm and 80 kHz is ~81 μm. Using this value for the initial bubble radius, the MATLAB codes applied to Eq. 1 calculated maximum wall velocities of 16, 26, and 34 m/s for low, medium, and high (0.01, 0.04, and 0.07 W/cm^2) acoustic intensities, respectively. These maximum wall velocities were then used in the following equations (25) to calculate the magnitude of the liquid shear rate around the oscillating bubble:

$$U_L = \frac{u_g^2}{2\pi f R_0}, \quad (4)$$

$$\delta = \left(\frac{\mu}{\pi\rho_L f}\right)^{\frac{1}{2}}, \quad (5)$$

and

$$G \cong \frac{U_L}{\delta}, \quad (6)$$

where u_g = velocity amplitude of bubble surface, U_L = streaming velocity, δ = velocity boundary layer thickness, G = velocity gradient (shear rate), and all other terms are as previously defined.

The calculated velocity gradients, or shear rates, are 6.6×10^6, 1.7×10^7, and 3.0×10^7 s^{-1} for low, medium, and high ultrasound intensities, respectively. To appreciate the extreme magnitude of these shear rates, the lowest shear rate is equivalent to the shear on fluid between plates separated by a 1-mm gap and having a differential velocity of 6600 m/s.

Previous studies have shown how liposomes deform under shear flow (30–34), but there is little work (32) that shows how liposomes might break up at high magnitudes of shear, and, more importantly, what their resulting size might be. Fortunately, a similar problem has been studied in the context of droplet emulsions undergoing shear (35) wherein the capillary number is used as the governing parameter. The capillary number (Ca) is the ratio of the shear forces (or other inertial forces) over surface tension forces, as shown by Eq. 7:

$$Ca = \frac{\text{Shear forces}}{\text{Surface tension forces}} = \frac{\mu G R^2}{SR} = \frac{\mu R G}{S}, \quad (7)$$

where R is the radius of curvature of the interface, and all other terms are as defined previously.

When a droplet is in a shear field, viscous shear forces tend to stretch the droplet, whereas surface tension forces tend to

keep it spherical. If the shear forces are much greater than surface tension, the drop elongates into an unstable cylinder and then breaks up into smaller drops, with smaller radii, which are subsequently subject to smaller shear forces. Drops continue to elongate and break up until they are sufficiently small that the surface tension forces keep them from elongating into unstable cylinders and then smaller drops. Thus, droplet size reduction continues until the elongation and restoring forces are balanced.

For lipid vesicles, the situation is a little different since the vesicle is not a homogenous droplet, but a lipid-covered solution. This will not change the fundamental forces experienced by the vesicle during shear, but may alter the stability and break up of the elongated cylinders. In contrast to stretched oil droplets, lipid tubes have several additional properties that could increase stability, including inherent curvature of different lipids, number of lipid molecules on the inner and outer leaflet, and the fixed ratio of surface area (lipids) to volume (trapped solution). The surface/volume ratio could be changed through water entry into the vesicle, but since there are membrane-impermeable ions in solution, osmotic forces prevent this. The surface/volume ratio is likely the most significant factor in lipid tube stability.

Previously, we obtained electrophysiological data consistent with formation of a small percentage of stable lipid tubes after sonication of lipid vesicles (36). Additionally, electron micrographs (EM) confirm the existence of lipid tubes and vesicles with extended tethers, even when fixed and stained several hours after sonication (20,36). However, these data are not convincing evidence in support of stable lipid tubes, since the electrophysiological data is indirect and tubes observed from EM may be artifacts of the fixing or staining process. To determine whether stable lipid tubes do form when subjected to ultrasound, we used RTM (Richardson Technologies; see Methods) to observe lipid suspensions 1 h after sonication (medium intensity at 1 atm). These observations were of vesicles in solution with a light microscope that had a resolution of ~200 nm. Fig. 5 shows several different images from RTM where lipid tubes were observed. These tubes are 3–15 times larger than the typical tube observed in EM, but we assume that tubes come in a range of sizes, and that RTM does not have the resolution to resolve smaller tubes. These structure of these larger tubes may be less common than that of the small tubes (and vesicles) observed in EM. Alternatively, the tubes observed using EM may be altered in size due to the fixation or staining process.

The RTM data confirm that tubes are sufficiently stable that some are still present after 1 h, but their presence does not reveal the nature of their stability. However, one fortuitous observation of a lipid tube with RTM sheds light on this question. As the tube was observed tumbling through solution, it suddenly stopped moving (suggesting that it had stuck to the glass slide) and rounded up into a sphere. This is consistent with the hypothesis that the tube is primarily stabilized by the fixed surface area/volume ratio, and that a small tear in the membrane allowed solute to enter and the tube to expand into a round vesicle (see Supplementary Material, Movie 1). Overall, stable tube formation after shear of lipid vesicles appears to be a relatively rare but predictable event.

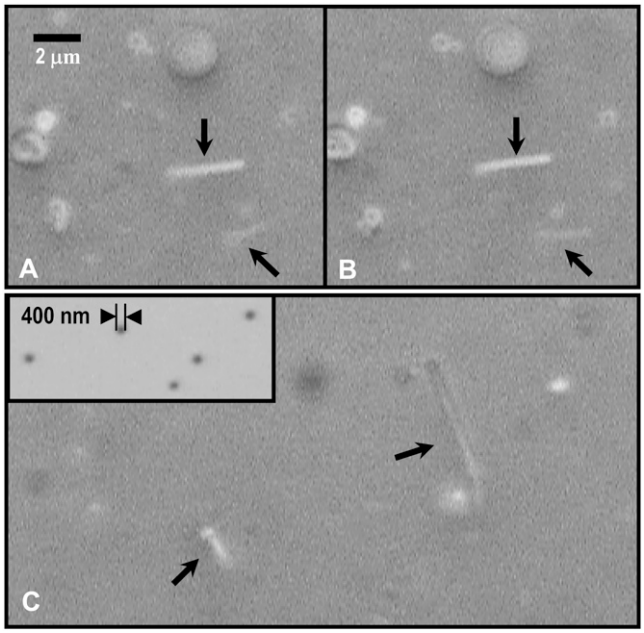

FIGURE 5 High resolution (RTM) images of sonicated lipid vesicles in solution. (*A*) Image showing two lipid tubes (*arrows*) among many large and small vesicles. Scale bar, 2 μm. (*B*) Same view as in *A*, but slightly later in time. Because the tubes are tumbling in space, different sections of the tubes are in focus at different times. (*C*) Another image of more lipid tubes and vesicles. (*Inset*) Calibration image of 404-nm polystyrene beads using the same optics. Moving images are presented in Supplementary Material.

In general, we assume that most shear elongation of liposomes creates unstable cylinders that break up into smaller liposomes. As an approximation, we can model a liposome subject to high shear rates as a droplet with an effective surface tension. Although there are limitations to this model, we can use the capillary number to explore the relationship between these two competing forces. When Ca is on the order of unity, the forces are balanced, and a critical radius can be calculated. A liposome with a radius less than the critical radius will remain intact without further reduction. Similar to a droplet, a liposome with a radius greater than the critical radius will be stretched by shear forces, and eventually break into liposomes with radii closer to or below the critical radius. Therefore, as more liposomes randomly enter into the small volume of the high shear field adjacent to oscillating bubbles, the population average of the liposome size would gradually approach a limit near the critical radius. The original population of larger liposomes would be depleted, and a smaller population protected by surface tension below the critical radius would increase and thus reduce the average liposome size as the sonication proceeded.

The size distribution that we observed in our samples supports this hypothesis. Samples that exhibited a decrease in effective diameter showed the presence of a bimodal population. We previously have studied the dynamics of these two populations and note that with sonication, the larger-diameter population is depleted, and the smaller-diameter liposomes become the dominant population (20).

Using a value of 3 dyn/cm (37,38) for the maximum surface tension of liposomes and previously determined values for the shear rate, the critical diameters for low-, medium-, and high-intensity ultrasound at 1 atm are 910, 350, and 200 nm, respectively. Assuming that liposomes with diameters above these values will be broken up and liposomes with diameters below these values will be preserved, they can be compared with the experimental results of Fig. 3. At 1 atm, the effective diameters after 1000 s of sonication are 240, 187, and 138 nm for low, medium and high intensities, respectively. Although these values differ by a factor of 2 to 4 from the simplified theoretical values, they are within the same order of magnitude and both follow the same trend (low intensity causes the least size change). The discrepancies might be attributed to the uncertainty in the value used for liposome maximum surface tension, which depends on phospholipid composition and sterol content, or perhaps on some of the assumptions of our model (e.g., bubble size, gas content, ''order-of-magnitude'' approximations made in deriving the microstreaming equations (26), and the critical capillary number being on the order of unity). In addition, even though microstreaming may be the primary mechanism of size reduction, it is likely that other noncavitational phenomena might be occurring, such as shock waves, thermal effects, etc.

The microstreaming model is supported by experimental results at higher static pressures as well. Equation 3 predicts that the resonant bubble radii at 2 and 4 atm are 57 and 80 μm, respectively. These bubble sizes and their corresponding static pressures were incorporated into the Rayleigh-Plesset equation, and the critical diameters for all static pressures and intensities, calculated from Eqs. 4–7, are shown in Fig. 6.

Fig. 6 shows the effects of both static pressure and acoustic intensity on calculated critical diameters. According to trends displayed in Fig. 3, static pressure and intensity play competing roles in determining the critical diameter above which liposomes are affected by the ultrasound. The smallest vesicles (smallest critical diameter) are formed at the lowest static pressure and highest acoustic intensity, whereas the largest vesicles are formed at high pressure and low intensity.

Table 2 indicates which samples are predicted to be unaffected by ultrasound according to the microstreaming model. If the critical diameter was above the average diameter of the sample before sonication (614 nm), it was labeled as ''unaffected''. These results correlate moderately well with the data in Fig. 3. All samples labeled ''unaffected'' did not change >21% of their original size, with one exception. The sample sonicated at low intensity and 1 atm was predicted to be unaffected yet had considerable size change. It is important to note that the critical diameter was found by assuming that breakup occurred when $Ca = 1$. In droplet emulsion applications, a critical Ca (not necessarily 1) must be experimentally determined before a critical diameter can be calculated. The uncertainty of the critical capillary number, along with approximations made in our calculations, still allows for size change under low intensity and 1 atm static pressure. The fact that the critical diameter is within the same order of magnitude as resulting daughter liposomes is strong evidence that the microstreaming is the responsible mechanism in manipulating liposome size. Furthermore, the model qualitatively explains the effects that intensity and static pressure have on this process.

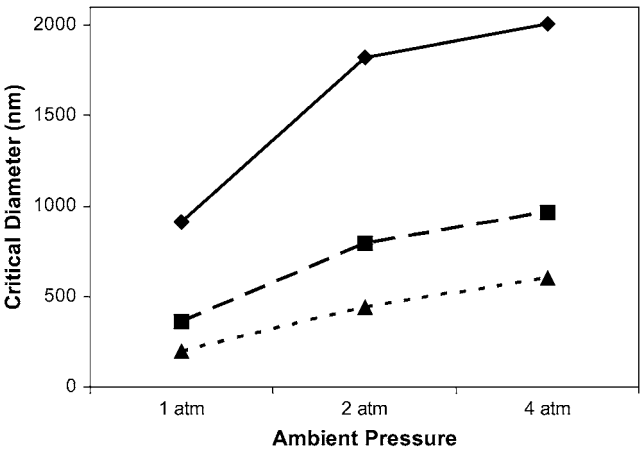

FIGURE 6 Critical diameters calculated as a function of both pressure and intensity. Both decreasing intensity (low, ♦; medium, ■; and high, ▲) and increasing ambient pressure raises the critical diameter. This is supported by trends in Fig. 3. The critical diameter is a limit above which liposomes may be more vulnerable to break apart by shear forces.

CONCLUSIONS

It appears that pressurization during sonication inhibits the decrease in liposome size, but increased intensity can counteract the inhibition. Furthermore, increased static pressure also inhibits the subharmonic and broadband emissions, but

TABLE 2 Prediction of the critical diameter of ultrasonically-sheared liposomes

Process conditions	1 atm	2 atm	4 atm
Low intensity	614 nm (unaffected)*	614 nm (unaffected)	614 nm (unaffected)
Medium intensity	350 nm	614 nm (unaffected)	614 nm (unaffected)
High intensity	200 nm	450 nm	610 nm

*Vesicle samples whose critical diameter is above the original effective diameter of the liposomes (614 nm) were labeled as ''unaffected''. Compare to the change in effective diameter shown in Fig. 3.

size change occurs even without either of these elements, and neither type of acoustic emission is correlated with liposome size change. Finally, our mathematical models show that stable (noncollapse) cavitation, always present with or without subharmonic or broadband emissions, can generate sufficient shear through acoustic microstreaming to reduce liposome size. These mathematical models of acoustic microstreaming can qualitatively explain the effects of pressure and acoustic intensity on liposome size reduction.

These observations and mathematical models support the hypothesis that it is microstreaming around oscillating bubbles, and not necessarily collapse cavitation events, that create shear sufficient to reduce the size of the liposomes during ultrasonic processing.

SUPPLEMENTARY MATERIAL

To view all of the supplemental files associated with this article, visit www.biophysj.org.

REFERENCES

1. Goyal, P., K. Goyal, S. G. V. Kumar, A. Singh, O. P. Katare, and D. N. Mishra. 2005. Liposomal drug delivery systems. Clinical applications. *Acta Pharm.* 55:1–25.
2. Litzinger, D. C., A. M. J. Buiting, N. Vanrooijen, and L. Huang. 1994. Effect of liposome size on the circulation time and intraorgan distribution of amphipathic poly(ethylene glycol)-containing liposomes. *Biochim. Biophys. Acta.* 1190:99–107.
3. Uhumwangho, M. U., and R. S. Okor. 2005. Current trends in the production and biomedical applications of liposomes: a review. *J. Med. Biomed. Res.* 4:9–21.
4. Woodbury, D. J., and C. Miller. 1990. Nystatin-induced liposome fusion. a versatile approach to ion channel reconstitution into planar bilayers. *Biophys. J.* 58:833–839.
5. Parente, R. A., and B. R. Lentz. 1984. Phase behavior of large unilamellar vesicles composed of synthetic phospholipids. *Biochemistry.* 23:2353–2362.
6. Hunter, D. G., and B. J. Frisken. 1998. Effect of extrusion pressure and lipid properties on the size and polydispersity of lipid vesicles. *Biophys. J.* 74:2996–3002.
7. Macdonald, R. C., R. I. Macdonald, B. P. M. Menco, K. Takeshita, N. K. Subbarao, and L. R. Hu. 1991. Small-volume extrusion apparatus for preparation of large, unilamellar vesicles. *Biochim. Biophys. Acta.* 1061:297–303.
8. Domazou, A. S., and P. L. Luisi. 2002. Size distribution of spontaneously formed liposomes by the alcohol injection method. *J. Liposome Res.* 12:205–220.
9. Huang, C. 1969. Studies on phosphatidylcholine vesicles. Formation and physical characteristics. *Biochemistry.* 8:344–352.
10. Lasic, D. D. 1988. The mechanism of vesicle formation. *Biochem. J.* 256: 1–11.
11. Lasic, D. D. 1987. A general model of vesicle formation. *J. Theor. Biol.* 124:35–41.
12. Fromherz, P., and D. Ruppel. 1985. Lipid vesicle formation. the transition from open disks to closed shells. *FEBS Lett.* 179:155–159.
13. Nyborg, W. L. 2001. Biological effects of ultrasound: development of safety guidelines. Part II: General review. *Ultrasound Med. Biol.* 27:301–333.
14. Brennen, C. E. 1995. Cavitation and Bubble Dynamics. Oxford University Press, New York.
15. Leighton, T. G. 1994. The Acoustic Bubble. Academic Press, London.
16. Leighton, T. G. 1989. Transient excitation of insonated bubbles. *Ultrasonics.* 27:50–53.
17. Delius, M. 1997. Minimal static excess pressure minimises the effect of extracorporeal shock waves on cells and reduces it on gallstones. *Ultrasound Med. Biol.* 23:611–617.
18. Sapozhnikov, O. A., V. A. Khokhlova, M. R. Bailey, J. C. Williams, J. A. McAteer, R. O. Cleveland, and L. A. Crum. 2002. Effect of overpressure and pulse repetition frequency on cavitation in shock wave lithotripsy. *J. Acoust. Soc. Am.* 112:1183–1195.
19. Franklin, M. J., W. S. A. Brusilow, and D. J. Woodbury. 2004. Determination of proton flux and conductance at pH 6.8 through single F-o sectors from *Escherichia coli*. *Biophys. J.* 87:3594–3599.
20. Woodbury, D. J., E. S. Richardson, A. W. Grigg, R. D. Welling, and B. H. Knudson. 2006. Reducing liposome size with ultrasound: bimodal size distributions. *J. Liposome Res.* 16:57–80.
21. Woodbury, D. J. 1999. Nystatin/Ergosterol method for reconstituting ion channels into planar lipid bilayers. *In* Methods in Enzymology, Vol. 294: Ion Channels, Part C. P. M. Conn, editor. Academic Press, San Diego. 319–339.
22. Morrison, I. D., E. F. Grabowski, and C. A. Herb. 1985. Improved techniques for particle-size determination by quasi-elastic light-scattering. *Langmuir.* 1:496–501.
23. Apfel, R. E., and C. K. Holland. 1991. Gauging the likelihood of cavitation from short-pulse, low-duty cycle diagnostic ultrasound. *Ultrasound Med. Biol.* 17:179–185.
24. Elder, S. A. 1958. Cavitation microstreaming. *J. Acoust. Soc. Am.* 31:54–64.
25. Nyborg, W. L. 1968. Mechanisms for nonthermal effects of sound. *J. Acoust. Soc. Am.* 44:1302–1309.
26. Nyborg, W. L. 1982. Ultrasonic microstreaming and related phenomena. *Br. J. Cancer.* 45:156–160.
27. Dyson, M. 1982. Nonthermal cellular effects of ultrasound. *Br. J. Cancer.* 45:165–171.
28. Wu, J. 2007. Shear stress in cells generated by ultrasound. *Prog. Biophys. Mol. Biol.* 93:363–373.
29. Phelps, A. D., and T. G. Leighton. 1997. The subharmonic oscillations and combination-frequency subharmonic emissions from a resonant bubble: Their properties and generation mechanisms. *Acta Acoustica.* 83:59–66.
30. Shahidzadeh, N., D. Bonn, O. Aguerre-Chariol, and J. Meunier. 1998. Large deformations of giant floppy vesicles in shear flow. *Phys. Rev. Lett.* 81:4268–4271.
31. Mendes, E., J. Narayanan, R. Oda, F. Kern, S. J. Candau, and C. Manohar. 1997. Shear-induced vesicle to wormlike micelle transition. *J. Phys. Chem. B.* 101:2256–2258.
32. Courbin, L., and P. Panizza. 2004. Shear-induced formation of vesicles in membrane phases: kinetics and size selection mechanisms, elasticity versus surface tension. *Phys. Rev. E.* 69:681031–681034.
33. de Haas, K. H., C. Blom, D. van den Ende, M. H. G. Duits, and J. Mellema. 1997. Deformation of giant lipid bilayer vesicles in shear flow. *Phys. Rev. E.* 56:7132–7137.
34. Abkarian, M., C. Lartigue, and A. Viallat. 2002. Tank treading and unbinding of deformable vesicles in shear flow: determination of the lift force. *Phys. Rev. Lett.* 88:2150401–2150412.
35. Cristini, V., S. Guido, A. Alfani, J. Blawzdziewicz, and M. Loewenberg. 2003. Drop breakup and fragment size distribution in shear flow. *J. Rheol.* 47:1283–1298.
36. Woodbury, D. J. 1989. Pure lipid vesicles can induce channel-like conductances in planar bilayers. *J. Membr. Biol.* 109:145–150.
37. Woodbury, D. J., and J. E. Hall. 1988. Role of channels in the fusion of vesicles with a planar bilayer. *Biophys. J.* 54:1053–1063.
38. Needham, D., and R. S. Nunn. 1990. Elastic-deformation and failure of lipid bilayer-membranes containing cholesterol. *Biophys. J.* 58:997–1009.